SCIENCE CHINA
Earth Sciences

SPECIAL TOPIC: Challenges and uncertainties of ENSO prediction: Enlightenments from El Niño event of 2015–2016 doi: 10.1007/s11430-017-9087-2
• RESEARCH PAPER •

On the "spring predictability barrier" for strong El Niño events as derived from an intermediate coupled model ensemble prediction system

QI QianQian[1,2], DUAN WanSuo[1,2*], ZHENG Fei[3] & TANG YouMin[4]

[1] *State Key Laboratory of Numerical Modeling for Atmospheric Sciences and Geophysical Fluid Dynamics, Institute of Atmospheric Physics, Chinese Academy of Sciences, Beijing 100029, China;*
[2] *University of Chinese Academy of Sciences, Beijing 100049, China;*
[3] *International Center for Climate and Environment Science, Institute of Atmospheric Physics, Chinese Academy of Sciences, Beijing 100029, China;*
[4] *Second Institute of Oceanology, State Oceanic Administration, Hangzhou 310012, China*

Received January 23, 2017; accepted July 13, 2017; published online August 8, 2017

Abstract Using predictions for the sea surface temperature anomaly (SSTA) generated by an intermediate coupled model (ICM) ensemble prediction system (EPS), we first explore the "spring predictability barrier" (SPB) problem for the 2015/16 strong El Niño event from the perspective of error growth. By analyzing the growth tendency of the prediction errors for ensemble forecast members, we conclude that the prediction errors for the 2015/16 El Niño event tended to show a distinct season-dependent evolution, with prominent growth in spring and/or the beginning of the summer. This finding indicates that the predictions for the 2015/16 El Niño occurred a significant SPB phenomenon. We show that the SPB occurred in the 2015/16 El Niño predictions did not arise because of the uncertainties in the initial conditions but because of model errors. As such, the mean of ensemble forecast members filtered the effect of model errors and weakened the effect of the SPB, ultimately reducing the prediction errors for the 2015/16 El Niño event. By investigating the model errors represented by the tendency errors for the SSTA component, we demonstrate the prominent features of the tendency errors that often cause an SPB for the 2015/16 El Niño event and explain why the 2015/16 El Niño was under-predicted by the ICM EPS. Moreover, we reveal the typical feature of the tendency errors that cause not only a significant SPB but also an aggressively large prediction error. The feature is that the tendency errors present a zonal dipolar pattern with the west poles of positive anomalies in the equatorial western Pacific and the east poles of negative anomalies in the equatorial eastern Pacific. This tendency error bears great similarities with that of the most sensitive nonlinear forcing singular vector (NFSV)-tendency errors reported by Duan et al. and demonstrates the existence of an NFSV tendency error in realistic predictions. For other strong El Niño events, such as those that occurred in 1982/83 and 1997/98, we obtain the tendency errors of the NFSV structure, which cause a significant SPB and yield a much larger prediction error. These results suggest that the forecast skill of the ICM EPS for strong El Niño events could be greatly enhanced by using the NFSV-like tendency error to correct the model.

Keywords 2015/16 strong El Niño event, Spring predictability barrier, Initial errors, Model errors

Citation: Qi Q Q, Duan W S, Zheng F, Tang Y M. 2017. On the "spring predictability barrier" for strong El Niño events as derived from an intermediate coupled model ensemble prediction system. Science China Earth Sciences, 60, doi: 10.1007/s11430-017-9087-2

1. Introduction

The El Niño-Southern Oscillation (ENSO) is the dominant inter-annual mode in the tropics and involves a strong inter-annual variation in sea surface temperature (SST) over the equatorial central-eastern Pacific. As a prominent climate phenomenon in the tropical coupled ocean-atmosphere system, ENSO has a strong effect on the global climate, the ecology

*Corresponding author(email: duanws@lasg.iap.ac.cn)

of the tropical Pacific and the economics of many countries across the globe. Hence, successful ENSO forecasts are essential for offering decision makers an opportunity to take into account anticipated climate anomalies (Ropelewski and Halpert, 1987; Trenberth et al., 1998). While ENSO theories and predictions have been greatly improved over recent decades, realistic ENSO predictions are still plagued by considerable uncertainties (Jin et al., 2008). In particular, the model prediction skill shows a sharp drop during boreal spring, regardless of the month during which the prediction begins. This phenomenon is called the "spring predictability barrier" (SPB), first suggested by Webster and Yang (1992).

The SPB is still a controversial problem in ENSO predictability studies. The SPB exists not only in ocean-atmosphere coupled dynamical models but also in statistical models (Kirtman et al., 2002). Statistically, the SPB manifests as a pronounced drop in the anomaly correction coefficient (ACC) between predicted and observed results across boreal spring (Webster and Yang, 1992; Latif et al., 1994; Webster, 1995; Lau and Yang, 1996; Torrence and Webster, 1998; Mc Phaden, 2003; Luo et al., 2008). From the perspective of error growth, the SPB refers to the phenomenon in which ENSO predictions often have a large prediction error; in particular, a prominent error growth usually occurs during spring and/or the beginning of summer when the predictions are made before and throughout the spring (Mu et al., 2007a, 2007b; Duan et al., 2009; Yu et al., 2009; Duan and Wei, 2012; Duan and Hu, 2015).

Various hypotheses have been formulated to explain the SPB. Some studies have emphasized the role of the climatological annual cycle and demonstrated that the weakest ocean-atmosphere coupling during boreal spring and a phase locking of the ENSO to the annual cycle induce the SPB for ENSO events (Zebiak and Cane, 1987; Webster, 1995; Balmaseda et al., 1994; Torrence and Webster, 1998). Xue et al. (1997a, 1997b) indicated that the occurrence of the SPB may arise from ENSO events themselves, showing that the SST anomalies (SSTA) for ENSO events in boreal spring are relatively small, making them difficult to detect and forecast in the presence of atmospheric and oceanic noise. Levine and McPhaden (2015) further emphasized the role of ENSO events and believed that the SPB is derived from the annual cycle of the ENSO growth rate. Ren et al. (2016) investigated the persistent barrier for ENSO events, which actually indicated the possible effect of ENSO events themselves on SPB. Clearly, these studies tend to suggest that the SPB is an inherent characteristic of ENSO predictions. Others, however, have emphasized the role of initial errors in the SPB. Chen et al. (1995, 2004) suggested that improving model initialization could greatly enhance the prediction skill of ENSO across spring. Mu et al. (2007a, 2007b) demonstrated that a particular initial error pattern, together with the effects of the climatological annual cycle and the El Niño event itself, causes a significant SPB. Furthermore, Mu et al. (2007b) showed that the initial errors with the structure of a conditional nonlinear optimal perturbation (CNOP; Mu et al., 2003) cause the most significant SPB, where the CNOP is the initial perturbation that satisfies a certain physical constraint and causes the largest perturbation growth at a certain prediction time. More recently, Yu et al. (2009) used the Zebiak-Cane model (Zebiak and Cane, 1987) and identified two types of CNOP-type initial errors associated with SPB: one possessing an SSTA pattern with negative anomalies in the equatorial central-western Pacific and with positive anomalies in the equatorial eastern Pacific and another with patterns nearly opposite to those of the former type (also see Duan et al., 2009). Duan and Wei (2012) and Yu et al. (2012) further found that CNOP-like initial errors also exist in the initial analysis fields of realistic ENSO predictions and produce much larger prediction errors. Therefore, if CNOP-type errors were filtered out from realistic ENSO predictions, the ENSO forecast skill would be greatly improved.

Model errors are another source of prediction errors. An increasing number of studies have indicated that model errors also affect the ability to predict ENSO (Wu et al., 1993; Hao and Ghil, 1994; Blanke et al., 1997; Flugel and Chang, 1998; Liu, 2002; Zhang et al., 2003; Zavala-Garay et al., 2004; Williams, 2005). With respect to the SPB, Yu et al. (2012) showed that model parametric errors do not cause a significant SPB for El Niño events. However, Duan and Zhao (2015) argued that model errors induce SPB for El Niño events when considering the combined effects of different types of model errors (also see Duan et al., 2016). Zheng and Zhu (2010) also suggested that reasonable consideration of model errors could alleviate the SPB effect on prediction uncertainties. These findings indicate that in addition to model parametric errors, uncertainties in other physical processes that can cause an SPB exist. In fact, Lopez and Kirtman (2014) found that including west wind bursting events (WWBs) in a prediction system significantly increases ENSO prediction skill compared with a prediction system that lacks WWBs; in the authors' case, an SPB was caused by the lack of WWB representation in the forecast system. Larson and Kirtman (2016) also demonstrated that persistent stochastic zonal wind stress perturbations near the equatorial dateline activate the coupled instability and suggested that stochastic wind stress perturbations are an important contributor to the SPB. Clearly, these studies have emphasized the role of model errors in yielding an SPB in El Niño events. Of course, whether the model errors produce a significant SPB in realistic predictions remains unknown.

As is well known, a strong El Niño event occurred in 2015. The event caused natural disasters in China, such as frequent, extreme torrential rain in the middle and lower reaches of the Yangtze River Basin in the summer of 2015 (Zhai et al., 2016). Many models have made forecasts of the 2015/16 El

Niño event and obtained relatively satisfactory skill scores. For example, the ENSO prediction system developed at the Beijing Climate Center (BCC) achieved a high skill score for its 2015/16 El Niño predictions (Ren et al., 2017). The intermediate coupled model ensemble prediction system (ICM EPS; Zheng et al., 2006, 2007), developed by the Institute of Atmospheric Physics, Chinese Academy of Sciences, successfully predicted the onset of the 2015/16 El Niño event and demonstrated high forecast skill (Zheng et al., 2016). Nevertheless, notable prediction uncertainties still exist, particularly for long lead times. We therefore ask: Is a significant SPB generated by the ICM EPS for 2015/16 El Niño predictions? If so, is it initial errors or model errors that play a more important role in causing the SPB phenomenon? What features of the initial errors and the model errors are associated with the SPB? To address these questions, we use the output of the ICM EPS to explore the SPB for the 2015/16 El Niño event and compare it with that obtained for other strong El Niño events such as the 1982/83 and 1997/98 El Niño events to investigate the characteristics of initial errors and/or model errors associated with the SPB from the perspective of error growth.

The remainder of the present paper is organized as follows. In the next section, we introduce the ICM EPS. In section 3, we describe the data used in this study and the forecast skill of the ICM EPS with respect to the 2015/16 El Niño event. The SPB for the 2015/16 El Niño forecasting generated by the ICM EPS is discussed in section 4, and the main source of the prediction errors associated with the SPB for the 2015/16 El Niño is revealed in section 5. In section 6, we illustrate the prominent characteristic of the model tendency error associated with the SPB for the 2015/16 El Niño event. In section 7, we demonstrate the tendency errors for the 1982/83 and 1997/98 El Niño predictions and provide useful suggestions. Finally, a summary and discussion are presented in section 8.

2. ICM EPS

The ICM EPS has three main components: an intermediate coupled model (ICM), an air-sea coupled data assimilation system, and a first-order linear Markov stochastic model. The ICM is an anomaly model developed by Keenlyside and Kleeman (2002) and Zhang et al. (2005). The model consists of a dynamical ocean model, an SST anomaly model that empirically parameterizes the temperature of subsurface water entrained into the mixed layer (T_e) based on sea level anomalies, and a statistical wind stress (τ) model. Specifically, the τ model is constructed from a singular value decomposition (SVD) of the covariance matrix calculated from time series of monthly mean SST and τ fields (see Syu et al., 1995; Chang et al., 2001); an inverse modeling method is adopted to estimate T_e anomalies using an SST anomaly equation, observed SST variability, and simulated mean and anomaly currents from the ocean model component. For further details, the readers are referred to the work of Zhang et al. (2005). The dynamical component of the ICM has been described by Keenlyside and Kleeman (2002), and thus the details are omitted here. The air-sea coupled data assimilation system (Zheng and Zhu, 2010, 2015) uses an ensemble Kalman filter (EnKF) approach to minimize the errors in both the atmospheric and oceanic initial conditions, where atmospheric wind stress, SST, and altimetry data are assimilated into the coupled model once per month through a coupled data assimilation approach (Zheng and Zhu, 2010). A first-order linear Markov stochastic model (Zheng et al., 2009a; Zheng and Zhu, 2016; also see the Appendix) is embedded within the ICM to perturb the modeled SST anomaly field randomly by adding error terms to the right-hand sides of the model equations. This stochastic model is designed to reduce model errors induced by the absence of westerly wind burst, Madden Julian Oscillation, etc. in the ICM (Zheng et al., 2006, 2009a, 2009b; Feng et al., 2015; Zheng and Zhu, 2016).

The performance of the ICM EPS has been documented by Zheng and Zhu (2016), whose 20-year retrospective forecast comparison showed that the EPS can achieve good forecast skill with a prediction lead time of up to one year; indeed, this forecast skill tends to be comparable with that of internationally popular coupled GCMs. Therefore, it is acceptable to use the predictions of this model to analyze the SPB for strong El Niño events, such as the 2015/16, 1997/98, and 1982/83 events.

3. Data and forecast skill of the ICM EPS with respect to the 2015/16 El Niño

3.1 The predicted and observed SSTA

The ENSO predictions used in this study are the monthly SSTAs for the 2015/16 El Niño event, which were generated by the ICM EPS. The ENSO predictions used consist of a leading 12-month ensemble forecast with 100 members for the 2015/16 El Niño, which was initialized from the 1st day of each month during the period from December 2013 to July 2015. The 100 members are obtained as follows. By integrating the ICM for five years by nudging the observed SST, physical variables with relatively dynamically balanced values are obtained. Using these values as initial values, we integrate the ICM coupled with the above-mentioned stochastic model 100 times and obtain 100 physical states with different values because of the stochasticity of the model. Using these 100 physical states, we apply the EnKF to assimilate the observations once per month to the initial field of the ICM coupled with the stochastic model and obtain 100 initial analysis fields for predictions. Thus, for each initial month, there is an ensemble forecast with 100 members, and for all initial months, a total of 2200 single forecasts (i.e., the sum of the

numbers of the ensemble forecast members at different initial months) are obtained. The meridional resolution of the ICM EPS outputs is 0.5º, covering 10ºS to 10ºN, and is gradually decreased to 3º from 10ºS to 31º S and from 10ºN to 31ºN; moreover, the zonal resolution is 2º, covering 124ºE to 30ºE. In the present study, we focus on the predictions for the tropical Pacific (31ºS–31º N, 124ºE–78ºW).

The available SST observations correspond to Extended Reconstructed Sea Surface (ERSSTv4; Smith et al., 2008) dates. The observations comprise a global monthly sea surface temperature dataset derived from the international Comprehensive Ocean-Atmosphere Dateset (ICOADS). The monthly analysis begins in January 1854, continuing to the present, and includes anomalies computed with respect to a 1971–2000 monthly climatology. The horizontal resolution is 2º ×2º, and the domain covers 89.0ºS to 89.0º N and 1.0º W to 359.5ºE.

The common spatial resolution and time span between the predictions and observations is highly convenient; therefore, we uniformly interpolate the horizontal resolution of both the predictions and observations as 1º×2º and take the time span to range from December 2013 to June 2016. To address the SPB for the 2015/16 El Niño event, we follow methods outlined in previous studies (Mu et al., 2007a, 2007b; Duan et al., 2009) to select the El Niño predictions with four start months in different seasons. Specifically, we select the start months 2014 (07) (i.e., July in year 2014), 2014 (10), 2015 (01) (i.e., January in year 2015), and 2015 (04), which fall during summer, autumn, winter, spring, respectively. Clearly, the leading 12-month forecasts with these selected start months pass through the spring of the growth phase of the 2015/16 El Niño event. We use Year (0) to denote the year when the El Niño event occurs, i.e., the year 2015, and Year (–1) and Year (1) to signify the years 2014 and 2016, respectively.

3.2 The forecast skill of the ICM EPS with respect to the 2015/16 El Niño event

To examine the prediction capability of the ICM EPS, in Figure 1 we present the predicted Niño-3.4 index for the 2015/16 El Niño events with different lead times, and in Figure 2 we present the correlations of the Niño-3.4 index between the mean of ensemble forecast members (hereafter as "ensemble-mean forecast") and the observations, where the anomalies, either in the model or in the observations, are calculated based on the climatological annual cycle generated by the SST over the period 1971–2000. The results show that the ICM EPS successfully predicts the occurrence of the

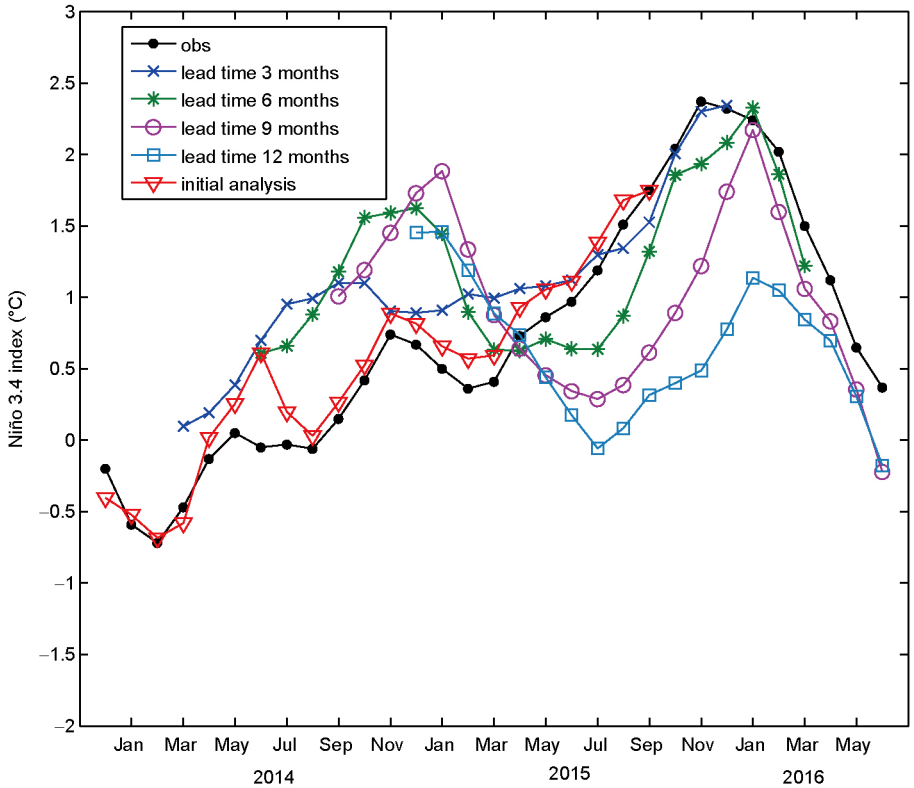

Figure 1 Monthly Niño-3.4 index for the 2015/16 El Niño derived from observations and predictions generated by the ensemble mean of the ICM EPS. The predictions involve an initial analysis, with leading 3-month, 6-month, 9-month and 12-month forecasts.

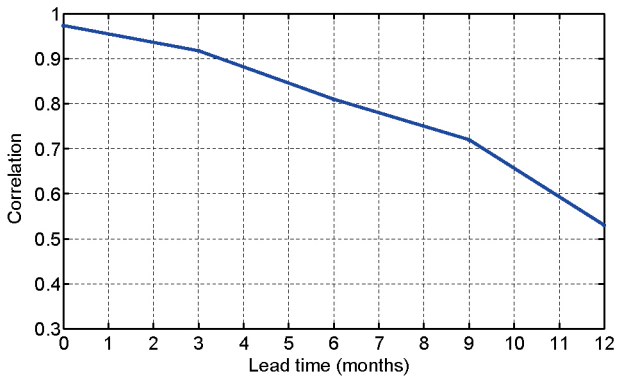

Figure 2 The prediction skill of the ensemble-mean forecasts shown in Figure 1. The skill is measured by the correlations between the predicted Niño-3.4 indices and the observed ones.

2015/16 El Niño. However, the correlations between the ensemble-mean forecasts and the observations decline with an increase in the lead time. Furthermore, the predicted peak time of the El Niño is 2−3 months later than the observed one, and the intensities are much weaker despite being comparable with the observations, particularly for relatively long lead times. Therefore, are these prediction uncertainties for the 2015/16 El Niño with long lead times caused by an SPB?

4. The SPB phenomenon for the 2015/16 El Niño event generated by the ICM EPS

Zheng and Zhu (2010) used the results of the ICM EPS to investigate the ENSO forecast skill by statistical analysis and observed the SPB phenomenon in a probabilistic sense. In this paper, we focus on the 2015/16 El Niño event to explore the SPB from the perspective of error growth and reveal the spatial characteristic of initial errors and/or model errors that cause a significant SPB.

The prediction errors are herein defined by the differences between the predictions and observations at prediction time t (i.e., lead time of predictions). Specifically, the prediction error $E(t)$ is expressed as follows:

$$E(t) = \|T^{\mathrm{p}}(t) - T^{\mathrm{o}}(t)\|_2 = \sqrt{\sum_{i,j}\left[T^{\mathrm{p}}_{i,j}(t) - T^{\mathrm{o}}_{i,j}(t)\right]^2}, \quad (1)$$

where T^{p} denotes the predicted SSTA, T^{o} represents the observed SSTA, and (i, j) are the grid points in the Niño-3.4 region; the norm $\|\|_2$ is used to measure the magnitude of prediction errors. The growth of the prediction errors is estimated by the growth tendency k of the prediction errors, which can be roughly evaluated by

$$k = \frac{\partial E(t)}{\partial t} \approx \frac{E(t_2) - E(t_1)}{t_2 - t_1}, \quad (2)$$

where $E(t_1)$ and $E(t_1)$ represent the prediction errors at future times t_1 and t_2, with $t_2 > t_1$, respectively; the future times t_1 and t_2 can occur at the beginning and end of a single month. A positive (negative) k value corresponds to an increase (decrease) in error, and the greater the absolute value of k is, the faster the increase (decrease) in error becomes.

To address the SPB for the 2015/16 El Niño events, we evaluate the prediction error of the SSTA for the 2015/16 El Niño and estimate its seasonal growth tendency, where the seasonal growth tendency is obtained by taking the sum of monthly growth tendencies k in one season but normalized by a factor of 3 (i.e., three months in one season). In Figure 3, we plot the mean of the seasonal growth tendency of the prediction errors for ensemble forecast members with start months 2014 (07), 2014 (10), 2015 (01) and 2015 (04). The prediction errors are time-dependent and are evaluated by eq. (1), with time t spanning from the starting month to the ending month of the predictions. The figure shows that the prediction errors tend to experience their largest growth rate in spring and/or summer (MJJ and/or JJA) and exhibit a significant season-dependent evolution, generating a significant SPB. We also plot the seasonal growth tendency of the prediction errors of the ensemble-mean forecast for SSTA in Figure 3. The figure shows that the results are similar. Furthermore, it is observed that for both the prediction errors of the ensemble-mean forecast and the mean of the prediction errors of the ensemble forecast members, much larger prediction errors occur with the 12-month lead time for the start month October than for the other start months (see Figure 4). To explore the reason for this discrepancy, in Figure 5 we plot the prediction errors for the 12-month leading predictions at each month. Mu et al. (2007a) demonstrated that the prediction errors for El Niño events often evolve in a manner similar to El Niño events themselves. That is, the prediction errors of the SSTA component for El Niño grow rapidly during spring and/or summer, peak in winter, and then decay. Figure 5 shows that the prediction errors for the 12-month leading predictions made in 2014 (07), 2015 (01), and 2015 (07) peak in winter but decay in the subsequent season, ultimately causing the prediction errors at the end of the 12-month lead time to be much smaller. However, the 12-month leading predictions made in 2015 (10) are practically initialized in winter in 2015 and do not persist to the next winter, which indicates that the corresponding prediction errors grow almost continuously throughout the entire forecast period and then become larger than those of the predictions made for other start months. In any case, Figures 3 and 4 show that the seasonal growth tendencies of the ensemble-mean prediction errors often tend to have smaller values than the mean of the seasonal growth tendencies of ensemble forecast members' prediction errors; furthermore, the former prediction errors at the prediction time (i.e., the end of the 12-month lead time) are much smaller. These results indicate that the SPB effect and the resulting prediction errors can be effectively reduced by an ensemble-mean forecast. As previously described, there were 100 ensemble forecast members at each start month, each of

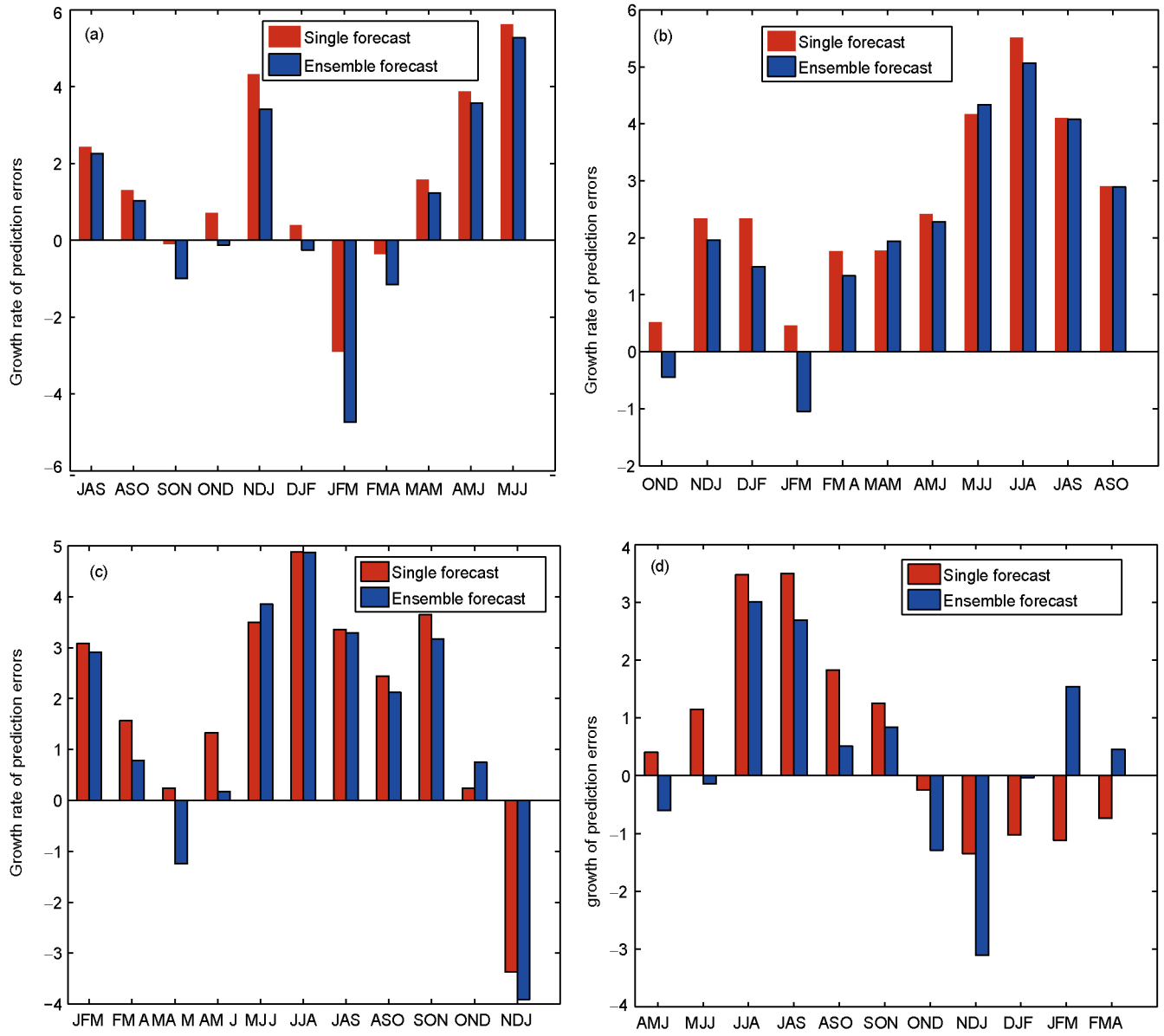

Figure 3 The mean of the seasonal error growth tendencies of the ensemble forecast members (red) and the seasonal error growth tendencies of the ensemble-mean forecast (blue), with the start months (a) 2014 (07), (b) 2014 (10), (c) 2015 (01), and (d) 2015 (04).

which was obtained by integrating the ICM coupled with the stochastic model with 100 initial analysis fields. It is clear that the prediction results for the 2015/16 El Niño events could be contaminated by both initial errors and model errors. Although the ICM was embedded with a stochastic model to reduce the effect of model errors, the randomness of the stochastic model may have induced new model errors. Furthermore, it is still likely to have other sources of model errors. These remaining model errors may be different among ensemble forecast members because of the randomness of the stochastic model. Therefore, we ask: Is it the initial or remaining model errors that are reduced to weaken the SPB effect in the 2015/16 El Niño predictions generated by the ICM EPS? This question is addressed in the next section.

5. Do initial or model errors determine the occurrence of the SPB for the 2015/16 El Niño event?

For the four start months adopted in the predictions (see section 4), there were a total of 400 predictions for the 2015/16 El Niño event. We now examine the contributions of these predictions to the SPB behavior. As defined in the introduction, the SPB refers to the phenomenon in which ENSO predictions have a large prediction error and prominent error growth during spring and/or the beginning of summer when the predictions are made before and throughout spring. By examining the prediction errors and the relevant seasonal growth tendency, we find that some predictions present significant error

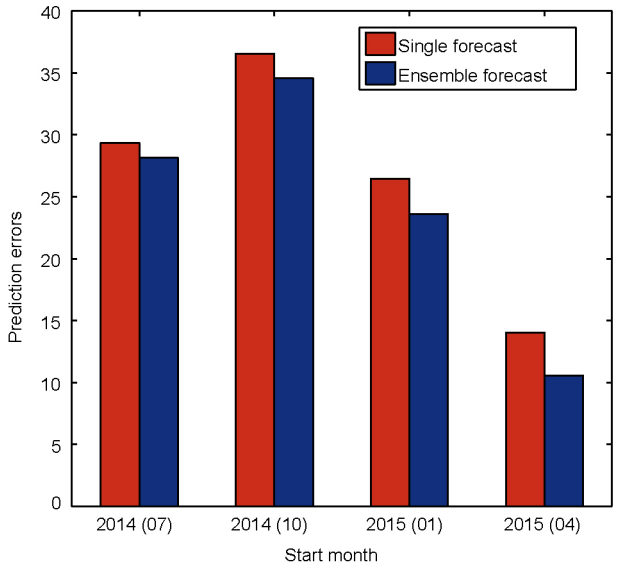

Figure 4 The mean of the prediction errors of the monthly Niño-3.4 SSTA for ensemble forecast members (red) and the prediction error of the monthly Niño-3.4 SSTA for ensemble-mean forecast (blue). The prediction errors are measured by the norm defined by eq. (1), where time t is the end of the 12-month lead time.

growth in spring and/or summer and make a significant contribution to a prominent SPB, whereas other predictions have negligible contributions because of either small error growth during the MJJ and JJA seasons or small prediction errors at the end of the 12-month lead time or both. Specifically, we show that 139 predictions make a significant contribution to the SPB and 261 predictions make a negligible contribution to the SPB (see Figure 6). For convenience, we refer to the former predictions as "SPB-related members" and the latter predictions as "non-SPB-related members".

As mentioned in the introduction, Mu et al. (2007a, 2007b) showed that the initial errors of a particular structure are more likely to cause SPB. In particular, Yu et al. (2009) and Duan et al. (2009) identified two types of initial tropical Pacific SSTA errors that cause a significant SPB for El Niño events. Thus, does the SSTA component of the initial analysis errors for the above-mentioned 139 SPB-related members also occur in different categories? To address this question, we perform a cluster analysis of these initial analysis errors, where the similarity coefficient is used to measure the similarities among initial error members. The similarity coefficient can be ex-

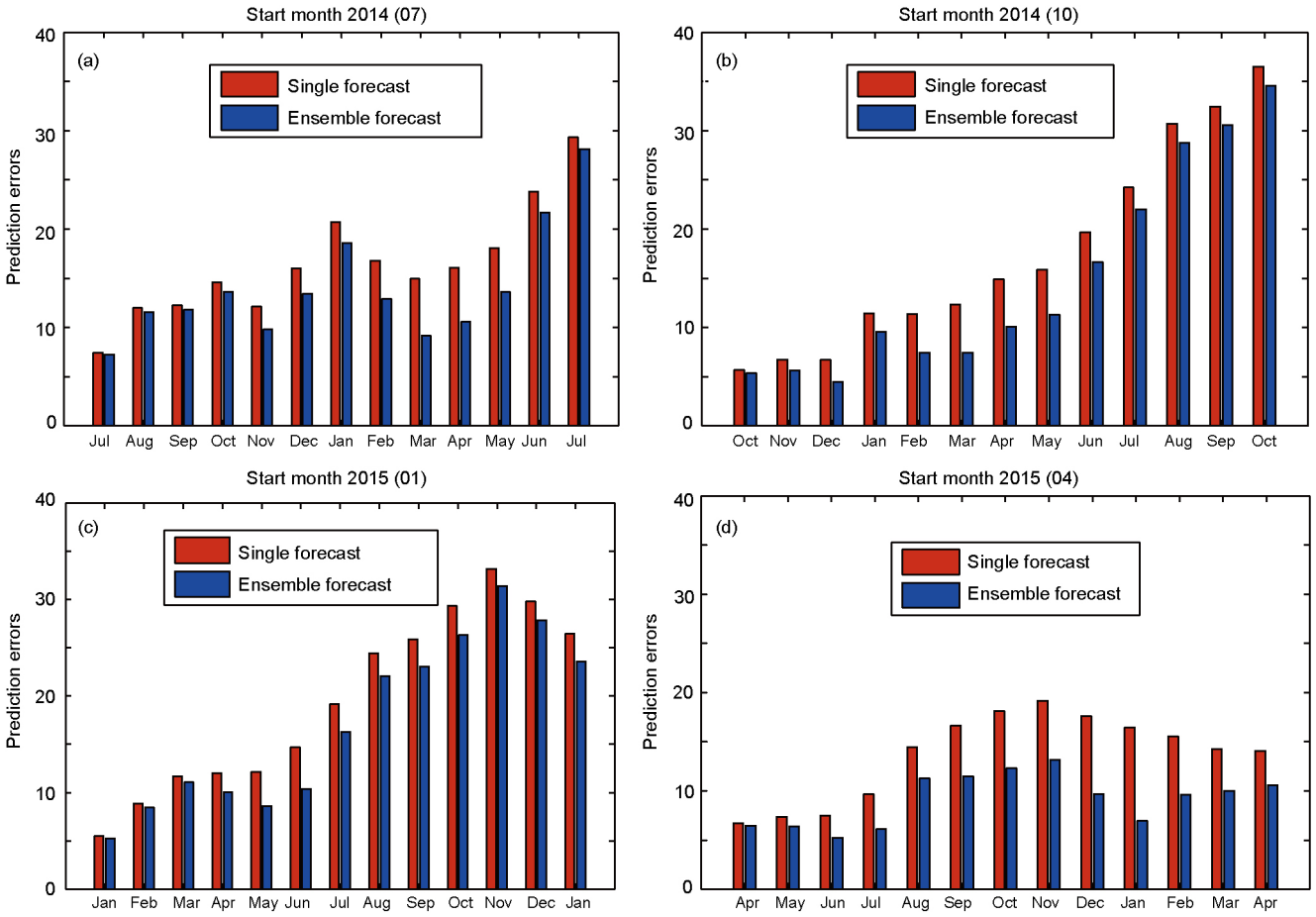

Figure 5 The mean of the prediction errors of the monthly Niño-3.4 SSTA for ensemble forecast members (red) and the prediction error of the monthly Niño-3.4 SSTA for ensemble-mean forecast (blue). The prediction errors are measured by the norm defined by eq. (1), where time t spans from the starting month to the ending month of the predictions.

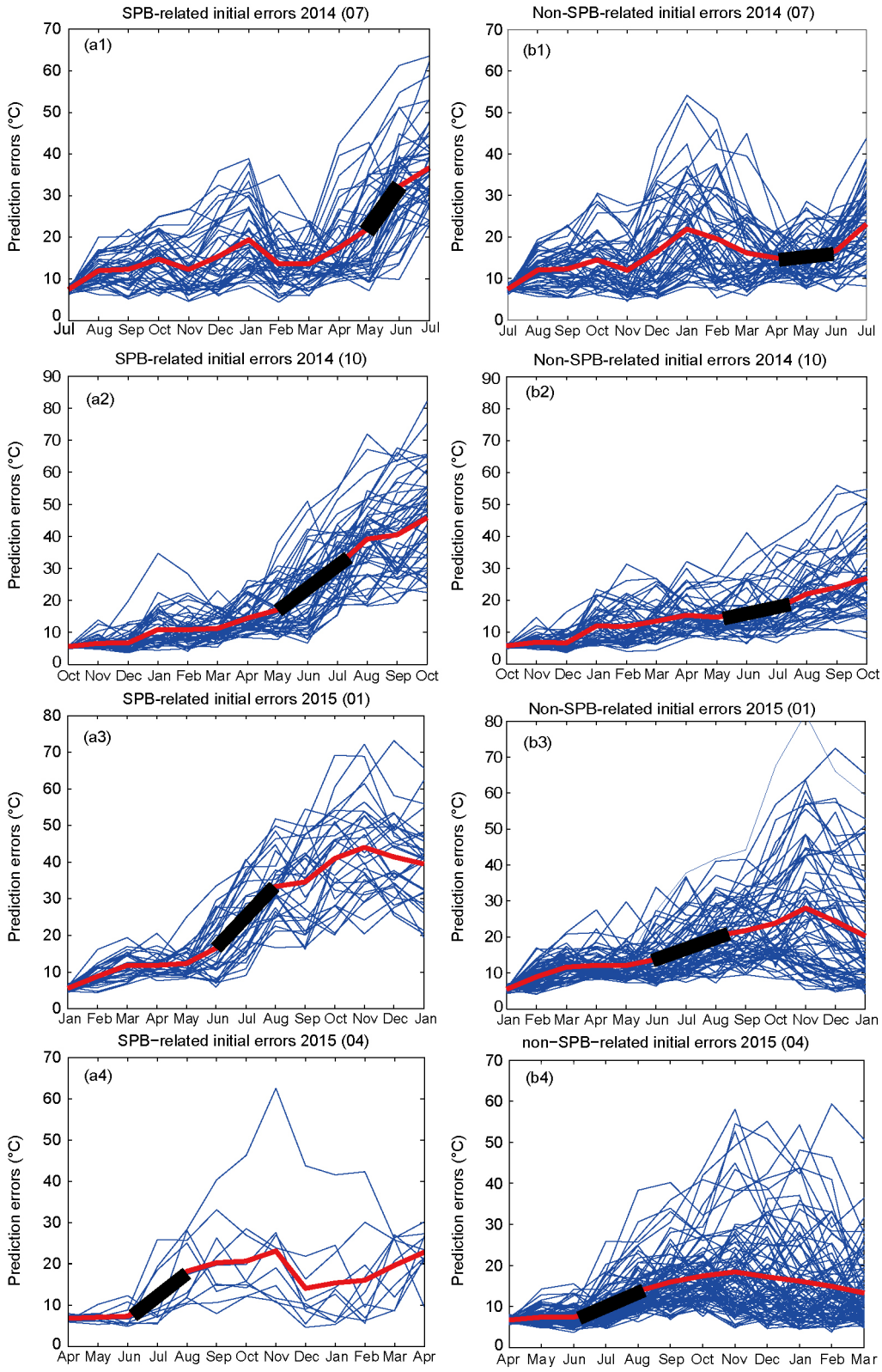

Figure 6 The evolution of the prediction errors (blue curves) for ensemble forecast members for the 2015/16 El Niño event, where the prediction errors are calculated by eq. (1), where time t spans from the start month to the end of the 12-month lead time. The left column shows the prediction errors of the SPB-related members, with start months (a1) 2014(07), (a2) 2014 (10), (a3) 2015 (01), and (a4) 2015 (04). The right column shows those associated with the non-SPB-related members, with the same start months indicated in the left column (i.e., b1–b4). The prediction errors associated with the SPB tend to present significant growth in spring and/or summer, which is indicated by the steep slopes (marked by the short, thick line) of the curves. The red curves represent the means of the prediction errors of the ensemble forecast members.

pressed as follows (Buizza, 1994; Kim et al., 2004):

$$s = \frac{< e_1, e_2 >}{\|e_1\|\|e_2\|}, \quad (3)$$

where e_i represents the ith initial error field, $< e_i, e_j >$ is the inner conduct of the initial errors e_i and e_j, and $\|e_i\| = < e_i, e_i >$, $i = 1, 2$. By calculating s of the initial SSTA errors over the region (10.5ºS–10.5ºN, 150ºE–90ºW), we classify the initial SSTA error for the 139 SPB-related members into four groups, with the group members' similarity coefficient being greater than 0.9 (Table 1). By observing these initial errors, it is surprising to find that these four groups of initial errors correspond precisely to the start months 2014 (07), 2014 (10), 2015 (01) and 2015 (04). We denote these groups of initial errors as "SPB_group-1", "SPB_group-2", "SPB_group-3", and "SPB_group-4", respectively. For convenience, we denote these groups of initial errors as "SPB-related initial SSTA errors".

For the 261 non-SPB-related members, we denote their initial SSTA errors as "non-SPB-related initial SSTA errors". We also use the cluster analysis approach to evaluate the similarity coefficients of the SSTA components and classify the non-SPB-related initial errors into four groups, with the group members' similarity coefficients greater than 0.9 (Table 2). These four groups of initial errors also correspond precisely to the four start months 2014(07), 2014(10), 2015(01) and 2015(04) and are denoted "non-SPB_group-1", "non-SPB_group-2", "non-SPB_group-3", and "non-SPB_group-4", respectively. When calculating the similarity coefficients of the SSTA components between the SPB-related initial errors and non-SPB-related initial errors at each start month, we find that they are also greater than 0.9. That is, the SSTA components for the SPB- and non-SPB-related initial errors at each start month bear great similarities (Table 3). It is inferred that the SPB for the 2015/16 El Niño that arises in the ICM EPS is not caused by the initial SSTA errors over the tropical Pacific. Is the SPB caused by the initial SSTA errors that occur in other oceanic regions or the initial errors arising from other physical variables? Zheng (2007) showed that if the ICM is not coupled with a first-order linear Markov stochastic model, the ensemble forecast members generated by the ICM and EnKF possess a small spread; however, the ensemble-mean forecast significantly deviates from the observations. Clearly, the deviation of the ensemble mean from the observation is mainly caused by model uncertainties. In the present study, we show that the initial tropical Pacific SSTA errors among the ensemble forecast members at each start month bear great similarities. From the small spread of the ensemble forecast members shown by Zheng (2007), it is inferred that, despite large errors in the SSTA component over other oceanic regions or in other physical variables, the predictions made by the ICM are less sensitive to these errors, which indicates that the ICM dynamics are much stable and contribute to the similarities among the initial analysis fields. In addition, the EnKF itself tends to reduce the background error covariance at the assimilation time and the initial analysis error covariance, thereby contributing to the similarities of the initial analysis fields (Evensen, 2003; Hamill et al., 2001). Therefore, although the ICM was coupled with the stochastic model, the EnKF itself, together with the stability of the model dynamics, tends to make the initial analysis fields bear similarities among themselves at the assimilation time. As a result, the reduction of the SPB of the ensemble-mean forecast possibly benefits from the decrease in the model errors.

Table 1 Similarity coefficients among four groups of SPB-related initial errors[a)]

	SPB_group-1	SPB_group-2	SPB_group-3	SPB_group-4
SPB_group-1	**0.9474**	0.5494	0.5004	0.5826
SPB_group-2	0.5494	**0.9440**	0.2350	0.4707
SPB_group-3	0.5004	0.2350	**0.9252**	0.3593
SPB_group-4	0.5826	0.4707	0.3593	**0.9522**

a) The values represent the averages of the correlations between all possible pairs within each group (bold) and from different groups (thin).

Table 2 Similarity coefficients among four groups of non-SPB-related initial errors[a)]

	non_SPB_group-1	non_SPB_group-2	non_SPB_group-3	non_SPB_group-4
non-SPB_group-1	**0.9475**	0.554	0.4996	0.565
non-SPB_group-2	0.554	**0.9434**	0.244	0.467
non-SPB_group-3	0.4996	0.244	**0.9171**	0.369
non-SPB_group-4	0.565	0.467	0.369	**0.9430**

a) The values are as defined in Table 1 but for non-SPB-related members.

Table 3 Similarity coefficients between SPB- and non-SPB-related initial errors

	Similarity coefficients
SPB_group-1 and non-SPB_group-1	0.9469
SPB_group-2 and non-SPB_group-2	0.9433
SPB_group-3 and non-SPB_group-3	0.9190
SPB_group-4 and non-SPB_group-4	0.9429

6. Which features of the model tendency error induce a significant SPB for the 2015/16 El Niño?

As demonstrated in section 5, the SPB of the 2015/16 El Niño event generated by the ICM EPS is mainly induced by the model error of the ICM. Then, which features of the model errors of the ICM induce a significant SPB? As is known, model errors may arise from uncertainties in physical parameterization processes or from the absence of physical processes such as westerly wind bursts or the Madden-Julian Oscillation. Therefore, the prediction errors caused by different types of model errors are mixed, and we cannot separate them precisely. With the Zebiak-Cane model (Zebiak and Cane, 1987), Duan et al. (2016) used the constant tendency errors to describe the combined effect of different types of model errors and adopted the nonlinear forcing singular vector approach (NFSV; Duan and Zhou, 2013) to identify the disturbing constant tendency errors that have the greatest effect on prediction uncertainties for El Niño events. Ultimately, the authors revealed two types of NFSV tendency errors: one type occurs during predictions through the growth phase of El Niño events and tends to present an SSTA pattern with positive anomalies in the equatorial central-western Pacific and negative anomalies in the equatorial eastern Pacific; the other type arises in predictions bestriding the decaying phase of El Niño events and has patterns nearly opposite to those of the former type. The model errors described by the two types of NFSV tendency errors illustrate the spatial structure of optimal model tendency errors, which may represent a type of model system error or the mean of different types of model errors during the forecast period. In the ICM EPS, although a stochastic model is embedded to reduce the model errors arising from the absence of westerly wind bursts, the Madden-Julian Oscillation, etc., uncertainties still exist in the ensemble-mean forecast for the 2015/16 events and even the SPB phenomenon (see previous sections), which indicates that model errors persist (including the random errors in the stochastic model). As previously mentioned, because of the interaction of the model errors from different sources, we cannot separate them precisely. Thus, in this section, we use the NFSV approach to extract the model errors represented by the tendency errors.

If we denote a state vector as U, the governing equations for U can be written as

$$\begin{cases} \dfrac{\partial U}{\partial t} = F(U(\boldsymbol{x}, t)), \\ U\big|_{t=0} = U_0, \end{cases} \quad in\ \Omega \times [0, \tau] \tag{4}$$

where $U_0(\boldsymbol{x}, t)$is the initial state $(\boldsymbol{x}, t) \in \Omega \times [0, \tau]$; Ω is a domain in R^n; t=0 is the initial time; $t = \tau$, with $\tau < +\infty$, is the future time of the evolution of the state variables; and F is a nonlinear operator. We assume that the dynamical system equation and the initial state are known exactly. For the future time $0 < t_n \le \tau$ and the corresponding state U_n, eq. (4) can be discretized as follows:

$$U_n = U_0 + \Delta t \sum_{i=0}^{n-1} F(U_i; t). \tag{5}$$

If one considers the effect of initial error on prediction results, eq. (5) can be written as follows:

$$U_n + u_n = U_0 + u_0 + \Delta t \sum_{i=0}^{n-1} F(U_i + u_i; t), \tag{6}$$

where u_0 is the initial error and u_n is the evolution of the initial error, i.e., the prediction error caused by the initial error. Moreover, if one only considers the effect of the model tendency error on the prediction results, then eq. (5) becomes

$$\begin{aligned} &U_n + u_n = U_0 + nf\,\Delta t + \Delta t \sum_{i=0}^{n-1} F(U_i + u_i; t), \\ &u_0 = 0, \end{aligned} \tag{7}$$

where f is the model tendency error. Comparing eq. (6) with eq. (7) clearly shows that the model tendency error can be equivalent to the initial error superimposed at each time step of the model integral when we assume that the model tendency error is constant. In fact, the model tendency error is time-dependent, but assuming a constant error may explain a type of time-independent model system error or the mean of time-dependent tendency errors. In any case, because one time step of the model integral is sufficiently short, the corresponding tendency error can be assumed to be constant. We use the tendency errors during each time step of the model integral to derive the constant tendency error for a forecast period. For one time step of the model integral, we write eq. (7) as follows:

$$\begin{aligned} &U_1 = U_0 + F(U_0; t)\Delta t, \\ &U_1 + u_1 = U_0 + u_0 + F(U_0 + u_0)\Delta t, \\ &U_1 + u_1 = U_0 + f\,\Delta t + F(U_0)\Delta t. \end{aligned} \tag{8}$$

In realistic predictions, the prediction results are often contaminated by both initial errors and model errors. Thus, the corresponding one-time-step forecast model can be written as

$$U_1 + v_1 = U_0 + u_0 + f\,\Delta t + F(U_0 + u_0; t)\Delta t, \tag{9}$$

where u_0 is the initial error as described in eqs. (6) and (8), f is the tendency error as described in eqs. (7) and (8), and v_1 is the prediction error caused by the initial error and tendency

error. According to eqs. (5) and (9), the tendency error f can be calculated as follows:

$$\begin{aligned} f &= \frac{U_1+v_1-U_0-u_0}{\Delta t} - F(U_0+u_0;t) \\ &= \frac{U_1+v_1-U_0-u_0}{\Delta t} - F(U_0) + F(U_0) - F(U_0+u_0) \\ &= \frac{U_1+v_1-U_0-u_0}{\Delta t} - \frac{U_1-U_0}{\Delta t} - [F(U_0+u_0)-F(U_0)] \\ &= \frac{v_1-u_0}{\Delta t} - [F(U_0+u_0)-F(U_0)]\,. \end{aligned} \tag{10}$$

From eqs. (8) and (10), it is clear that the first term on the right-hand side of eq. (10) is the growth tendency of the prediction error caused by the initial error and tendency error and the second term represents the growth tendency of the prediction errors caused by the initial errors. That is, the tendency error f can be deduced by subtracting the tendency of the prediction errors caused by the initial error from those caused by the initial error and tendency error.

We have classified ensemble forecast members for the 2015/16 El Niño event into two groups: 139 SPB-related members and 261 non-SPB-related members (see Section 4). Moreover, the SPB of the ICM EPS with respect to the 2015/16 El Niño forecasts is mainly induced by model errors, which can be described by the model tendency error. Now, we use the 139 SPB-related and the 261 non-SPB-related members to extract the tendency errors that often induce the SPB for the 2015/16 El Niño event according to eq. (10). Specifically, we sort the members of each group in descending order of the magnitudes of the prediction errors. We select the first 139 SPB-related members and the last 139 non-SPB-related members and take the difference between the two groups of members, thus obtaining 139 time-dependent time series with a lead time of 12 months. According to eq. (10), it is easily inferred that, because the two groups of forecast members have highly similar initial errors, the values of the 139 time-dependent times series practically alleviate the effect of the initial errors and thus only include the remaining prediction errors associated with the model errors. It is conceivable that these remaining prediction errors characterize the prediction errors that induce the SPB for the 2015/16 El Niño event. Therefore, we may further extract the prominent characteristic of the tendency errors that often induce an SPB for the 2015/16 El Niño events based on the remaining prediction errors using eq. (10).

When the remaining time-dependent prediction errors are related to eq. (10), it is observed that they only involve their growth tendency (i.e., the first term of eq. (10)) because they have filtered the effect of initial errors and excluded the second term of eq. (10). Furthermore, the growth tendency of the remaining prediction errors can be easily calculated because the associated prediction errors v and initial errors u_0 are known. The prominent characteristic for the SPB-related tendency error f can then be easily extracted by computing the first term on the right-hand side of eq. (10). Indeed, we evaluate the first term of eq. (10) for the remaining time-dependent prediction errors at each month of the 12-month prediction period and obtain 12 monthly tendency errors f. To extract the constant tendency error, we take the mean of the 12 monthly tendency errors for each of the 139 time-dependent remaining prediction errors and obtain 139 patterns for the tendency errors. By applying the EOF analysis method, we detect the first EOF mode of the 139 tendency errors (responsible for 48% of total variance; see Figure 7). The EOF1 and its PC1 indicate that most of ensemble forecast members tend to have positive values of PC1 and thus present tendency error patterns similar to those of the EOF1 mode. In fact, such tendency errors indicate an SSTA cooling rate over the tropical Pacific and illustrate the prominent characteristic of the tendency errors that often cause an SPB for the 2015/16 strong El Niño event forecasts generated by the ICM EPS. Such tendency errors induce anomalous easterly wind stress over the tropical Pacific and under-predict the strength of the El Niño event, which may explain why the 2015/16 El Niño forecast with a 12-month lead time tended to be under-predicted (see Figure 1).

Figure 7 demonstrates that the tendency errors of the EOF1 mode often induce an SPB in 2015/16 El Niño predictions generated by the ICM EPS and cause those forecasts to under-predict the strength of the event. However, it cannot be the tendency error that causes the most significant SPB or, in particular, the largest prediction error for the 2015/16 El Niño event, as indicated by the NFSV-tendency error. To determine the spatial characteristics of the tendency errors that cause the largest prediction error, we mainly address the members that have large prediction errors among the 139 SPB-related forecast members. Eq. (10) shows that the prediction errors v are involved in the first term of eq. (10). Furthermore, the first term was calculated for each forecast member when we estimated the dominant mode of the SPB-related tendency errors shown in Figure 7. For convenience, we directly use the modes indicated by the first term of eq. (10) (i.e., the growth tendency of prediction errors caused by initial errors and model errors) to identify the members that have the largest prediction errors. For the 139 SPB-related forecast members, there are 139 time-dependent series of prediction errors caused by initial errors and model errors. For each of these 139 series of prediction errors, we can calculate the growth tendency of the prediction error during each month and yield 12 growth tendencies. By taking the mean of these 12 growth tendencies, we obtain 139 patterns for the growth tendency for the 139 SPB-related forecast members. By performing an EOF analysis of these 139 growth tendency patterns, we obtain the first three EOF modes and their opposite modes, which account for 84.9% of the total variance (see Figure 8). We denote these six modes as EOF_1+, EOF_1–, EOF_2+, EOF_2-, EOF_3+, EOF_3–, respectively. For the

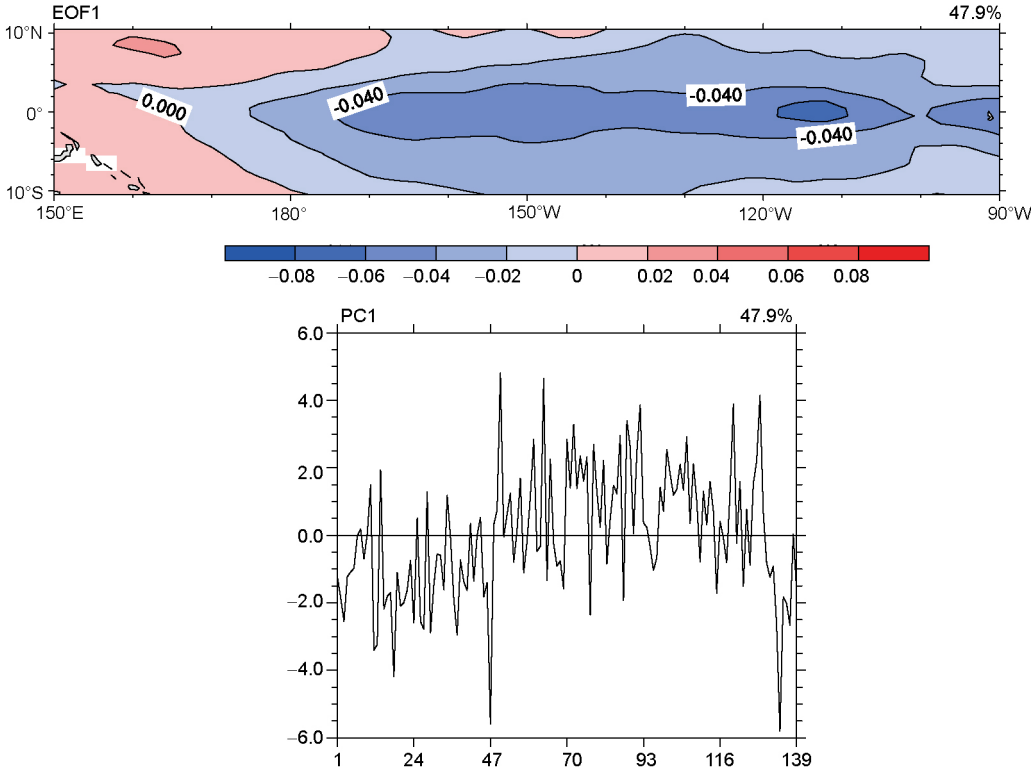

Figure 7 The first EOF mode and its PC1 of the 139 tendency errors. The EOF1 pattern is for the SSTA component (unit: ºC/month). Each number located on the horizontal axis in PC1 represents one of the 139 tendency errors, which correspond to the 139 SPB-related forecast members. For example, the number 70 corresponds to the 70th forecast member.

139 SPB-related forecast members, we select the members whose growth tendencies of the prediction errors are highly correlated (including positively and negatively correlated) with EOF_1+, EOF_2+, EOF_3+, respectively. If the PC amplitudes of the forecast members are larger than the mean value of the positive PC of all members, we believe that these members are highly positively correlated with the corresponding EOF pattern. Conversely, if the PC amplitudes of the members are smaller than the mean value of the negative PC of all members, these members are considered highly negatively correlated with the negative pattern of the corresponding EOF pattern. For the members that are highly positively or negatively correlated with EOF_1+, EOF_2+, and EOF_3+, we calculate the prediction errors for SSTA over the Niño 3.4 region at the end of the 12-month lead time; the results are illustrated in Figure 9. The figure shows that the prediction errors of the ensemble forecast members whose prediction error growth tendencies are of the EOF_3+ mode are the largest ones.

We also obtain the members that present the lowest prediction error among the non-SPB-related forecast members. We subtract the members with the lowest prediction error among the non-SPB-related forecast members from those with the largest prediction error among the SPB-related forecast members. The remaining prediction error therefore alleviates the effect of initial errors and mainly reflects the prediction errors associated with model errors. Similarly to the calculation described by Figure 7, we use these remaining prediction errors to obtain the tendency errors that cause a significant SPB and, in particular, the largest prediction errors for the 2015/16 El Niño. The results show that the tendency error presents a large-scale dipolar pattern with the east dipole of negative anomalies in the equatorial eastern Pacific and the west dipole of positive anomalies in the equatorial western Pacific (Figure 10).

7. The tendency errors for the 1982/83 and 1997/98 El Niño event forecasts

It is known that the years 1982/83 and 1997/98 also presented strong El Niño events similar to the 2015/16 El Niño. Naturally, we ask whether the results obtained for these events are similar to those obtained for the 2015/16 event. To this end, we use the hindcast results for the 1982/83 and 1997/98 El Niño events generated by the ICM EPS (Zheng et al., 2009a) and conduct a predictability analysis similar to that performed for 2015/16 El Niño. As expected, the two events yield results similar to those obtained for the 2015/16 event. For simplicity, we describe the results but do not provide the details. Specifically, the ICM EPS produces an SPB for predictions

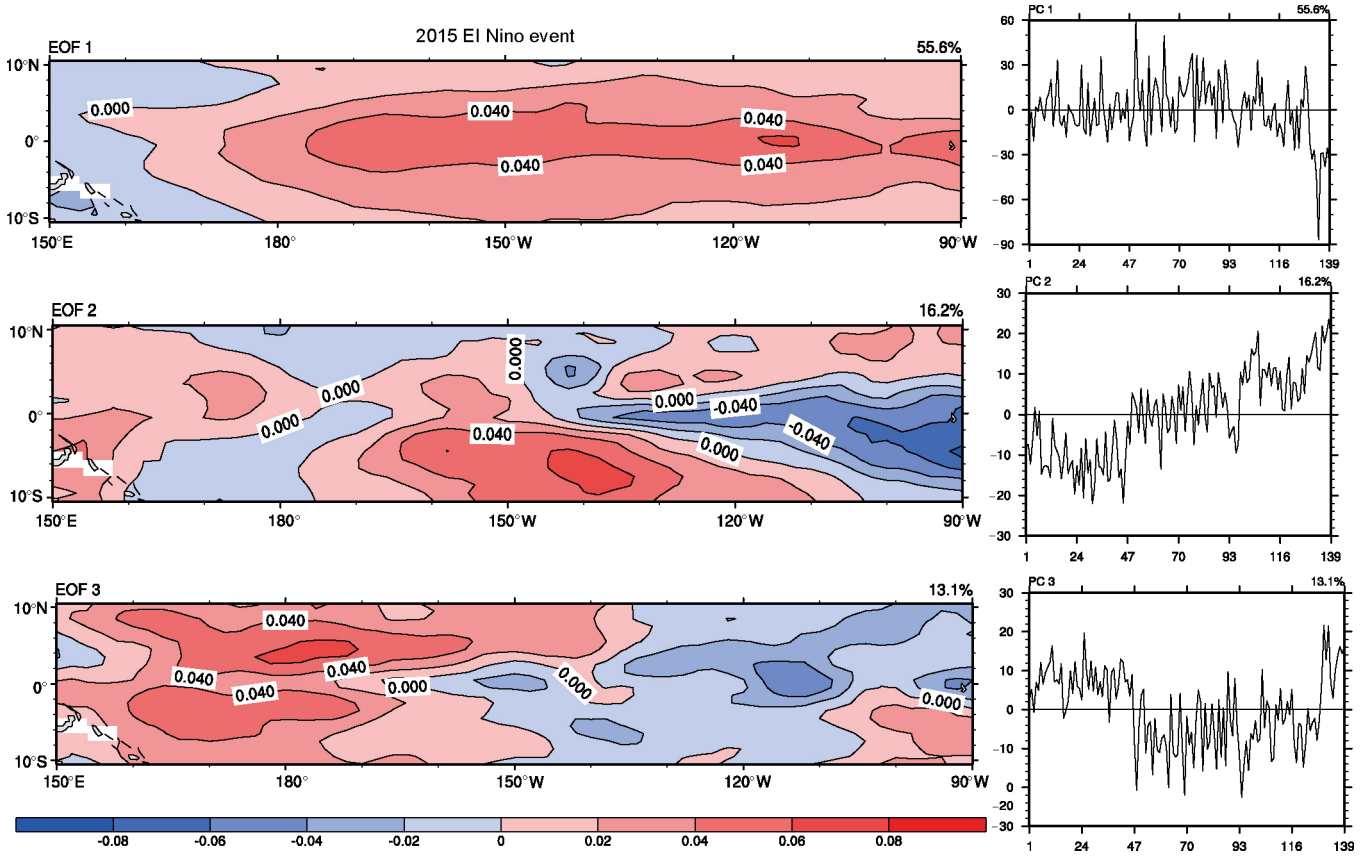

Figure 8 The first three EOF modes and their PCs of the 139 growth tendencies of prediction errors. The EOF patterns are for the SSTA component (Unit: ºC/month). The numbers located on the horizontal axis in PCs represent the 139 growth tendencies of prediction errors, which correspond to the 139 SPB-related forecast members. For example, the number 70 corresponds to the 70th forecast member.

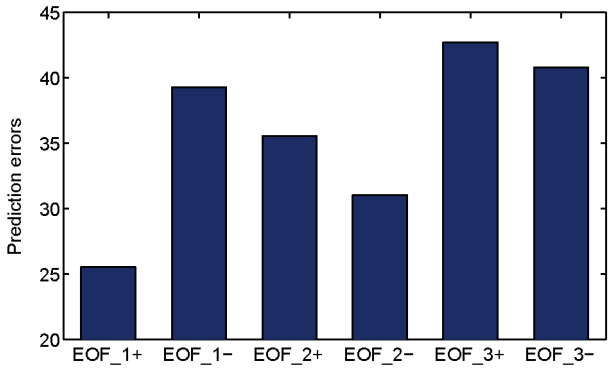

Figure 9 The prediction errors with growth tendencies of the modes EOF_1+, EOF_1–, EOF_2+, EOF_2-, EOF_3+, and EOF_3–, which are estimated by eq. (1), where time *t* is the end of the 12-month lead time.

of the 1982/83 and 1997/98 El Niño events and under-predicts their intensities; it is mainly the model errors of the ICM that limit the forecast skill for these two events. By applying eq. (10), we extract the dominant mode of the constant tendency errors for the two El Niño forecasts (Figure 11). It is illustrated that the dominant tendency error mode presents a pattern similar to that of the 2015/16 event, i.e., the pattern in which the SSTA cooling rate covers the tropical Pacific. As discussed in section 6, such a pattern could induce an anomalous easterly wind and cause SSTA cooling, thus explaining the under-prediction of the 1982/83 and 1997/98 El Niño events.

In addition, we also identify the prominent characteristic of the tendency errors that cause a significant SPB and, in particular, the largest prediction error for the 1982/83 and 1997/98 El Niño events. Specifically, we calculate the EOF modes of the constant tendency errors for the SPB-related forecasting members and, according to these EOF modes, classify the SPB-related forecasting members into different groups. The group whose members have the largest prediction errors are then identified by comparing the prediction errors between different groups. For non-SPB-related forecasting members, we take the members with the lowest prediction errors and subtract them from those with the largest prediction errors among the SPB-related forecast members. We then compute the growth tendency of these remaining prediction errors at each month and take the time mean of the growth tendency as the constant tendency error, as in eq. (10). Thus, two tendency error patterns are obtained, which show the prominent characteristics of the ICM's tendency errors that cause a significant SPB and the largest prediction error for the 1982/83

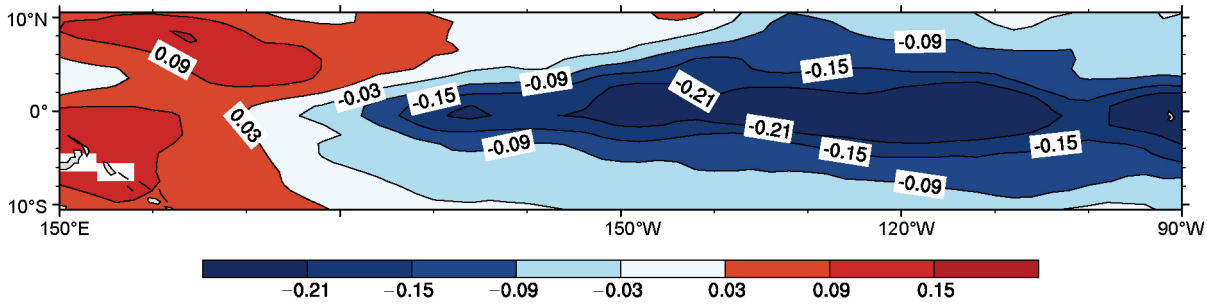

Figure 10 The tendency error pattern that emphasizes the prominent characteristic of the tendency errors that yield a significant SPB and, in particular, the largest prediction error for the 2015/16 El Niño event.

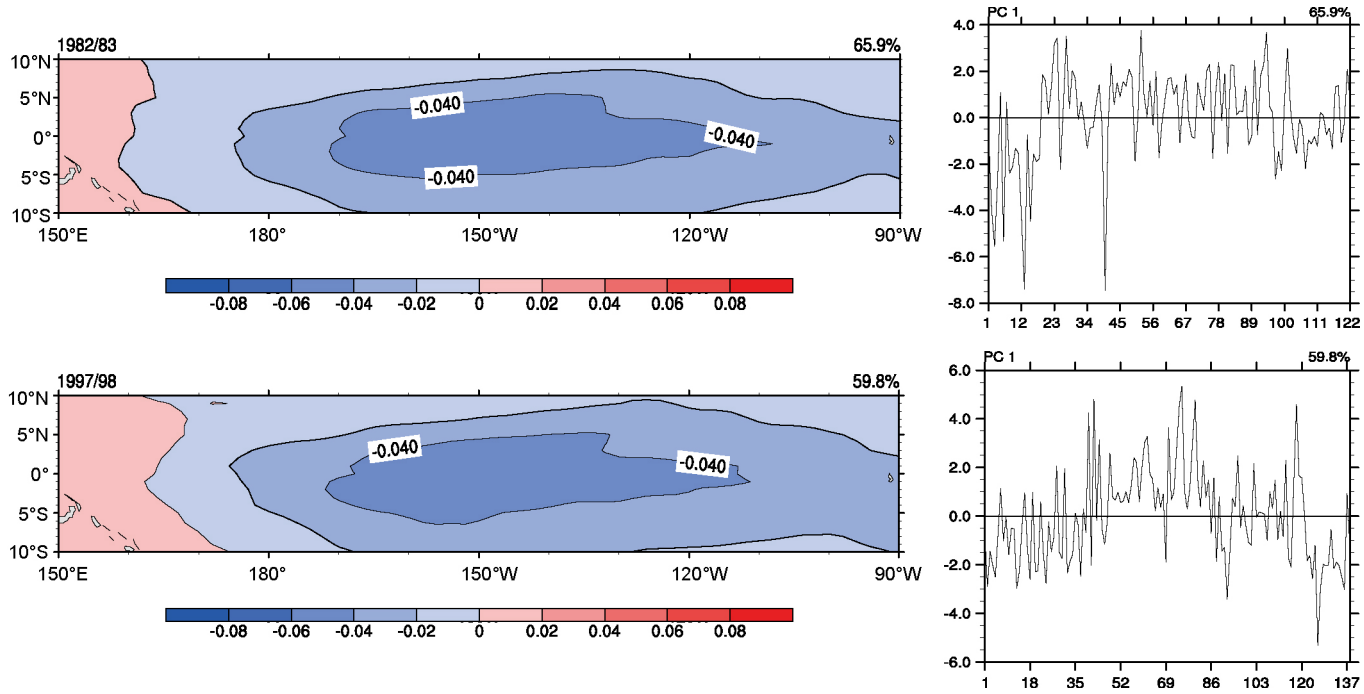

Figure 11 The first EOF modes and the corresponding PC1s of the tendency errors that often cause an SPB for the 1982/83 El Niño event (top) and the 1997/98 El Niño event (bottom). The EOF patterns are for the SSTA component (Unit: ºC/months). The numbers located on the horizontal axis in PC1s represents the forecast members that give rise to an SPB.

and 1997/98 El Niño events (see Figure 12). It is clear that such tendency errors for either the 1982/83 or 1997/98 El Niño event are very similar to that for the 2015/16 El Niño and show a large-scale dipolar pattern with an east dipole of negative anomalies and a west dipole of positive anomalies, except that the locations of the diploes depend on the El Niño events. These tendency errors bear great resemblance to the nonlinear forcing singular vector (NFSV; Duan and Zhou, 2013) tendency errors of the Zebiak-Cane model (Zebiak and Cane, 1987) reported by Duan et al. (2016). The NFSV tendency error represents the tendency error that causes the largest prediction error for El Niño events and demonstrates the sensitivity of the prediction error for El Niño events to model errors. The present results indicate that the NFSV tendency error for El Niño events also exists in realistic El Niño predictions generated by the ICM EPS and that this error corresponds not only to a significant SPB but also larger prediction errors. As previously mentioned, the NFSV tendency error can be understood as a type of model system error or the mean of different types of model errors during the forecast period. The NFSV-like tendency errors obtained indicate that the mean of different types of model errors for the ICM during the forecast period is not equal to zero. It is therefore reasonable to suggest that if one corrects the ICM by adding the opposite pattern of the NFSV-like tendency error to the SSTA tendency equation of the ICM, the ENSO forecast skill could be enhanced.

8. Discussion and summary

In this study, we first use ICM EPS outputs to investigate the SPB problem for the 2015/16 El Niño event. The results show that the ensemble forecast members often present a significant SPB for the 2015/16 El Niño predictions, as does the ensem-

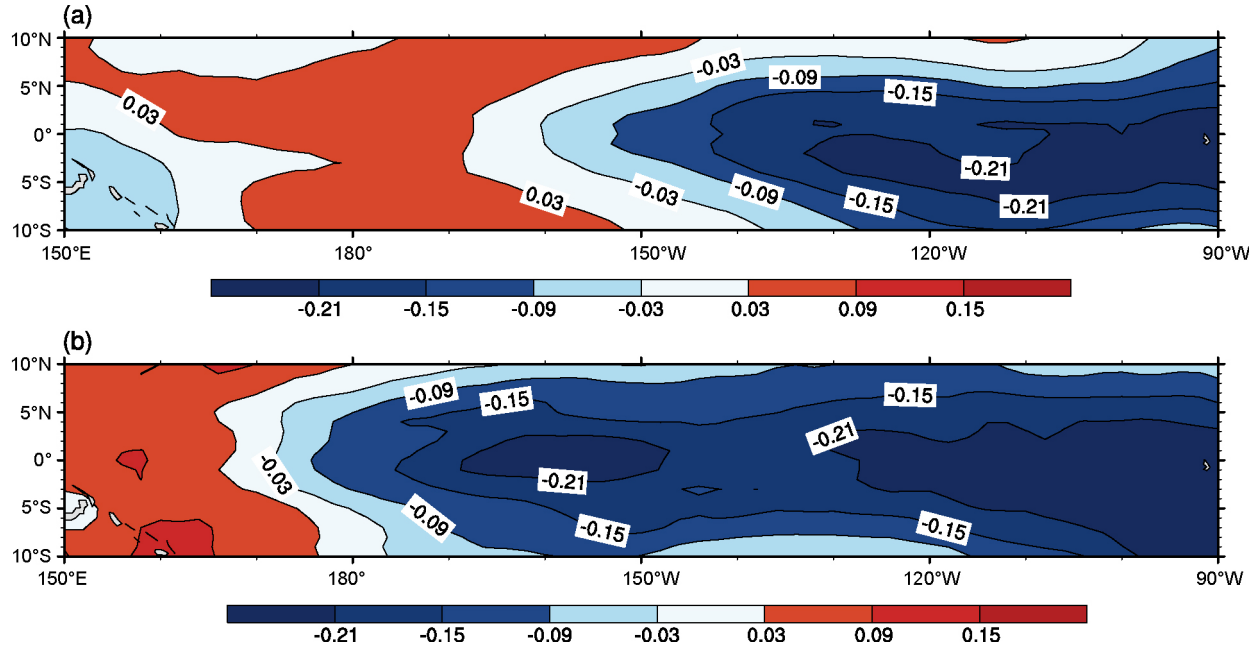

Figure 12 The tendency error pattern that emphasizes the prominent characteristic of the tendency errors that yield the largest prediction error and a significant SPB for the (a) 1982/83 and (b) 1997/98 El Niño events

ble-mean forecast. Nevertheless, the latter shows a much weaker SPB and smaller prediction error, implying that the uncertainties in ensemble forecasts are clearly reduced by taking the ensemble mean. Furthermore, because the initial SSTA fields of the ensemble forecast members for the ICM EPS generated by the EnKF bear very high similarities and the ICM is not sensitive to initial perturbations, we conclude that it is mainly the ICM's model errors and not the initial errors that cause a significant SPB for the 2015/16 El Niño event. It is conceivable that the small prediction error of the ensemble-mean forecast is due to the ensemble mean filtering the effect of model errors. Because the ICM, as mentioned in section 2, includes a linear and first-order Markov stochastic model to correct the predicted SSTA, different ensemble forecast members might involve different model errors because of the randomness of the Markov model. The model errors may show different spatial structures for different ensemble forecast members. Furthermore, some ensemble forecast members present a significant SPB, while others cause a less significant SPB or fail to show a SPB. These results indicate that model errors with certain structures are much more likely to cause a significant SPB than others. Following Duan et al. (2016), the present study uses tendency errors to describe model errors and reveal the prominent characteristic of the tendency errors of the ICM (coupled with the stochastic model) that cause a significant SPB and the largest prediction error for the 2015/16 El Niño event. Specifically, these tendency errors present a large-scale dipolar pattern of the SSTA component, with the east dipole of negative anomalies in the equatorial eastern Pacific and the west dipole of positive anomalies in the equatorial western Pacific, similar to a La Niña mature phase pattern.

For the historical 1982/83 and 1997/98 El Niño events, we obtain similar results and show that the tendency errors that give rise to a significant SPB and the largest prediction error are associated with a large-scale dipolar pattern of the SSTA component, with an east dipole of negative anomalies and a west dipole of positive anomalies, which bear resemblance to the pattern of the 2015 El Niño and are highly similar to the most sensitive NFSV tendency error (of the Zebiak-Cane model) for El Niño predictions reported by Duan et al. (2016). These findings imply that the NFSV tendency error reported by Duan et al. (2016) also exists in realistic predictions for the El Niño event. The NFSV errors represent the most sensitive tendency errors for predictions. That is, the NFSV tendency errors cause large prediction errors. Because the ICM tendency errors that give rise to a significant SPB for strong El Niño events are similar to the NFSV tendency errors and cause the largest prediction errors, the prediction skill of the ICM EPS for strong El Niño events could be enhanced if one uses the opposite pattern of the SPB-related tendency errors to constrain the SST tendency equation and reduce the model errors.

Mu et al. (2007a, 2007b) demonstrated that the initial errors can cause a significant SPB for ENSO events. Moreover, Yu et al. (2009) and Duan et al. (2009) presented the specific pattern of the initial errors that is most likely to cause an SPB for El Niño events (also see Duan and Wei, 2012, Mu et al., 2014, Duan and Hu, 2015, and Hu and Duan, 2016). In the present study, we showed that the model errors of the ICM induce an SPB for the 2015/16, 1982/83, and 1997/98 strong El Niño events. That is, the present study illustrates an example

of El Niño predictions in which model errors can also yield an SPB for El Niño events furthermore, model tendency errors of a particular pattern could be much more likely to cause a significant SPB for the strong El Niño events than other errors.

The ICM EPS adopted the EnKF to yield ensemble initial perturbations and attempted to achieve the appropriate diversity of ensemble forecast members and an acceptable forecast skill for ENSO events. However, the different ensemble forecast members, as demonstrated in the present study, possess initial SSTA fields with great similarities and small spread. This situation is not favorable for yielding the large but appropriate ensemble spread that is extremely useful for estimating the prediction uncertainties of ensemble forecasts. However, the ICM EPS showed a certain ensemble spread and acceptable forecast skill for the above-mentioned strong El Niño events. In fact, it is the linear and stochastic Markov model embedded in the ICM that perturbs each ensemble forecast member and thereby causes the ensemble forecast members to possess great diversity and present a much larger spread. If we were to adopt other approaches, such as the orthogonal CNOPs proposed by Duan and Huo (2016), to yield the ensemble forecast members, would the ICM EPS produce a greater diversity of ensemble forecast members even if it does not use the linear and stochastic Markov model to correct itself? In this case, can we draw the conclusion that the model errors induce the SPB for the strong El Niño events predicted by the ICM EPS? These questions are challenging but important for improving the forecast skill of the ICM EPS and deserve to be explored further.

Appendix

To reduce the simulation deficiencies of coupled air-sea interactions and subsurface thermal effects in the ICM, Zheng et al. (2007) proposed a linear and first-order Markov stochastic model (see eq. (A1)) for describing the model uncertainties at different prediction times and forced the ICM (see eq. (A2)) to reduce the effect of model errors. The first-order Markov stochastic model describes the evolution of the model errors over time and is expressed as follows.

$$\begin{aligned} Q_j^{(t)} &= \sum_{i=1}^{M} \sigma_{i,j} \times T_{i,j}^{(t)} \times U_{i,j}(x,y) + \xi_j^{(t)} \\ T_{i,j}^{(t)} &= \alpha_{i,j} \times T_{i,j}^{(t-1)} + \sqrt{1-\alpha_{i,j}^2} \times w_{i,j}^{(t)} \\ \xi_j^{(t)} &= \sigma_{resid,j} \cdot \zeta_j^{(t)}(x,y)\,. \end{aligned} \tag{A1}$$

In eq. (A1), $U_{i,j}$ represents the spatial pattern of the ith EOF mode for the SSTA component of the model error Q at time t in the jth month of the lead time and has a particular horizontal distribution, where the model error Q is obtained by estimating the root mean square errors between the deterministic forecast results and the observations along the lead time. $T_{i,j}^{t}$ represents the normalized coefficient of the ith EOF mode at time t in the jth month, where the coefficient $\alpha_{i,j}$ is the correlation between the ith mode in the jth month and that in the j+1th month, and $w_{i,j}^{t}$ is a random number of the ith mode at the time t, with a mean equal to 0 and a variance equal to 1. $\sigma_{i,j}$is the standard deviation of the model errors represented by the ith mode in the jth month. $M$is the number of EOF modes used in the stochastic model. To achieve reasonable model error amplitudes, the first 10 EOF modes are used in the stochastic model. Eq. (A1) then ensures that the variance in $T_{i,j}^{t}$ is equal to 1 as long as the variance of $T_{i,j-1}^{t}$ is equal to 1, which ultimately produces a sequence of time-correlated pseudorandom fields with the mean equal to zero and variance equal to 1. ξ_j^t represents a residual random field for Q at time t, where $\sigma_{resid,j}$is the standard deviation of the residual field obtained by removing the first M EOF modes from the observation-minus-forecast values, and $\zeta_j^{(t)}(x,y)$ is white noise drawn from the pseudorandom fields at time t, with the distribution of the mean equal to 0 and the variance equal to 1.

If one step integral of the ICM numerical model can be simply denoted by $\psi^{(t)} = f(\psi^{(t-1)})$, then the ICM coupled to the stochastic model can be expressed by combining eqs. (A1) and (A2).

$$\psi^{(t)} = f(\psi^{(t-1)}) + \sqrt{\Delta t}\, Q_j^t, \tag{A2}$$

where $\psi^{(t)}$represents the model states at time t, f is the numerical model propagator, Δt is the time step of the model integral, and Q_j^trepresents the model errors at time t in the jth month of the lead time.

To construct the above-mentioned stochastic model, Zheng et al. (2016) identified the first and second EOF modes (i.e., U in eq. (A1)) for the SST anomaly component of the model errors Q at lead times of 1, 4, 7, and 10 months. The model uncertainties indicated by the first EOF mode are located over the eastern equatorial Pacific, and as the lead time increases, these uncertainties extend to the central equatorial Pacific, finally presenting a canonical El Niño-like evolving mode; by contrast, the model uncertainties indicated by the second EOF mode are mainly concentrated in the North Pacific and the upturning region of South America and may reflect the model errors arising from coupled air-sea interactions and subsurface thermal effects.

Acknowledgements *This work was supported by the National Natural Science Foundation of China (Grant Nos. 41230420 & 41525017) and the National Public Benefit (Meteorology) Research Foundation of China (Grant No. GYHY201306018).*

References

Balmaseda M A, Anderson D L T, Davey M K. 1994. ENSO predictability using a dynamical ocean model coupled to a statistical atmospheres. Tellus-A , 46: 497–511

Blanke B, Neelin J D, Gutzler D. 1997. Estimating the effect of stochastic wind stress forcing on ENSO irregularity. J Clim, 10: 1473–1486
Buizza R. 1994. Sensitivity of optimal unstable structures. Q J R Met Soc, 120: 429–451
Chang P, Ji L, Saravanan R. 2001. A hybrid coupled model study of tropical Atlantic variability. J Clim, 14: 361–390
Chen D, Zebiak S E, Busalacchi A J, Cane M A. 1995. An improved procedure for EI Nino forecasting: Implications for predictability. Science, 269: 1699–1702
Chen D, Cane M A, Kaplan A, Zebiak S E, Huang D. 2004. Predictability of El Niño over the past 148 years. Nature, 428: 733–736
Duan W S, Liu X C, Zhu K Y, Mu M. 2009. Exploring the initial errors that cause a significant "spring predictability barrier" for El Niño events. J Geophys Res, 114: doi: 10.1029/2008JC004925
Duan W S, Wei C. 2012. The 'spring predictability barrier' for ENSO predictions and its possible mechanism: Results from a fully coupled model. Int J Clim, 33: 1280–1292
Duan W S, Zhao P. 2015. Revealing the most disturbing tendency error of Zebiak-Cane model associated with El Niño predictions by nonlinear forcing singular vector approach. Clim Dyn, 44: 2351–2367
Duan W, Hu J. 2015. The initial errors that induce a significant "spring predictability barrier" for El Niño events and their implications for target observation: Results from an earth system model. Clim Dyn, 46: 3599–3615
Duan W, Huo Z. 2016. An approach to generating mutually independent initial perturbations for ensemble forecasts: Orthogonal conditional nonlinear optimal perturbations. J Atmos Sci, 73: 997–1014
Duan W, Zhao P, Hu J, Xu H. 2016. The role of nonlinear forcing singular vector tendency error in causing the "spring predictability barrier" for ENSO. J Meteorol Res, 30: 853–866
Duan W, Zhou F. 2013. Non-linear forcing singular vector of a two-dimensional quasi-geostrophic model. Tellus A-Dyn Meteor Oceanogr, 65: 18452
Evensen G. 2003. The ensemble Kalman filter: Theoretical formulation and practical implementation. Ocean Dyn, 53: 343–367
Evensen G. 2004. Sampling strategies and square root analysis schemes for the EnKF. Ocean Dyn, 54: 539–560
Flugel M, Chang P. 1998. Does the predictability of ENSO depend on the seasonal cycle? J Atmos Sci, 55: 3230–3243
Feng L, Zheng F, Zhu J, Liu H. 2015. The role of stochastic model error perturbations in predicting the 2011/12 double-dip La Niña. SOLA, 11: 65–69
Hamill T M, Whitaker J S, Snyder C. 2001. Distance-dependent filtering of background error covariance estimates in an ensemble Kalman filter. Mon Wea Rev, 129: 2776–2790
Hao Z, Ghil M. 1994. Data assimilation in a simple tropical ocean model with wind stress errors. J Phys Oceanogr, 24: 2111–2128
Hu J Y, Duan W S. 2016. Relationship between optimal precursory disturbances and optimally growing initial errors associated with ENSO events: Implications to target observations for ENSO prediction. J Geophys Res, 121: doi: 10. 1002/2015JC011386
Jin E K, Kinter Iii J L, Wang B, Park C K, Kang I S, Kirtman B P, Kug J S, Kumar A, Luo J J, Schemm J, Shukla J, Yamagata T. 2008. Current status of ENSO prediction skill in coupled ocean-atmosphere models. Clim Dyn, 31: 647–664
Keenlyside N, Kleeman R. 2002. On the annual cycle of the zonal currents in the equatorial Pacific. J Geophys Res, 107: doi: 10. 1029/2000JC0007111
Kim H M, Morgan M C, Morss R E. 2004. Evolution of analysis error and adjoint-based sensitivities: Implications for adaptive observations. J Atmos Sci, 61: 795–812
Kirtman B P, Shukla J, Balmaseda M, Graham N, Penland C, Xue Y, Zebiak S. 2002. Current status of ENSO forecast skill: A report to the Climate Variability and Predictability Numerical Experimentation Group. CLIVAR Working Group on Seasonal to Interannual Prediction. Clim. Variability and Predictability, Southampton Oceanogr. Cent., Southampton, UK
Latif M, Barnett T P, Cane M A, Flügel M, Graham N E, von Storch H, Xu J S, Zebiak S E. 1994. A review of ENSO prediction studies. Clim Dyn, 9: 167–179
Lau K M, Yang S. 1996. The Asian monsoon and predictability of the tropical ocean-atmosphere system. Q J R Meteorol Soc, 122: 945–957
Larson S M, Kirtman B P. 2016. Drivers of coupled model ENSO error dynamics and the spring predictability barrier. Clim Dyn, 48: 3631–3644
Levine A F Z, McPhaden M J. 2015. The annual cycle in ENSO growth rate as a cause of the spring predictability barrier. Geophys Res Lett, 42: 5034–5041
Liu Z. 2002. A simple model study of ENSO suppression by external periodic forcing. J Clim, 15: 1088–1098
Lopez H, Kirtman B P. 2014. WWBS, ENSO predictability, the spring barrier and extreme events. J Geophys Res Atmos, 119: 10114–10138. doi: 10.1002/2014JD021908
Luo J J, Masson S, Behera S K, Yamagata T. 2008. Extended ENSO predictions using a fully coupled ocean-atmosphere model. J Clim, 21: 84–93
Mc Phaden M J. 2003. Tropical Pacific Ocean heat content variations and ENSO persistence barriers. Geophys Res Lett, 30: 319–338
Mu M, Duan W S, Wang B. 2003. Conditional nonlinear optimal perturbation and its applications. Nonlin Processes Geophys, 10: 493–501
Mu M, Duan W, Wang B. 2007a. Season-dependent dynamics of nonlinear optimal error growth and El Niño-Southern Oscillation predictability in a theoretical model. J Geophys Res, 112: D10113
Mu M, Xu H, Duan W S. 2007b. A kind of initial errors related to "spring predictability barrier" for El Niño events in Zebiak-Cane model. Geophys Res Lett, 34: doi: 10.1029/2006GL-27412
Mu M, Yu Y, Xu H, Gong T. 2014. Similarities between optimal precursors for ENSO events and optimally growing initial errors in El Niño predictions. Theor Appl Climatol, 115: 461–469
Ropelewski C F, Halpert M S. 1987. Global and regional scale precipitation patterns associated with the El Niño/Southern Oscillation. Mon Wea Rev, 115: 1606–1626
Ren H L, Jin F F, Song B, Lu B, Tian J Q, Zuo Y, Liu J, Wu C B, ZhaoY, Nie P Q, Zhang J B, Yu J, Wu J H, WanY P, Yan F Z. 2017. Prediction of Primary Climate Variability Modes at the Beijing Climate Center. J Meteor Res, 31: 204–223
Ren H L, Jin F F, Tian B, Scaife A A. 2016. Distinct persistence barriers in two types of ENSO. Geophys Res Lett, 43: 10973–10979
Smith T M, and Reynolds R W. 2004. Improved Extended Reconstruction of SST 1854–1997. J Clim, 17: 2466–2477
Smith T M, Reynolds R W, Peterson T C, Lawrimore J. 2008. Improvements NOAAs historical merged land-ocean temp analysis (1880–2006). J Clim, 21: 2283–2296
Syu H H, Neelin J D, Gutzler D. 1995. Seasonal and interannual variability in a hybrid coupled GCM. J Clim, 8: 2121–2143
Torrence C, Webster P J. 1998. The annual cycle of persistence in the El Niño Southern Oscillation. Q J R Meteorol Soc, 124: 1985–2004
Trenberth K E, Branstator G W, Karoly D, Kumar A, Lau N C, Ropelewski C. 1998. Progress during TOGA in understanding and modeling global teleconnections associated with tropical sea surface temperatures. J Geophys Res, 103: 14291–14324
Webster P J, Yang S. 1992. Monsoon and Enso: Selectively interactive systems. Q J R Met Soc, 118: 877–926
Webster P J. 1995. The annual cycle and the predictability of the tropical coupled ocean-atmosphere system. Meteorl Atmos Phys, 56: 33–55
Williams P D. 2005. Modelling climate change: The role of unresolved processes. Philos Trans R Soc A-Math Phys Eng Sci, 363: 2931–2946
Wu D H, Anderson D L T, Davey M K. 1993. ENSO variability and external impacts. J Clim, 6: 1703–1717
Xue Y, Cane M A, Zebiak S E. 1997a. Predictability of a coupled model of

ENSO using singular vector analysis. Part I: Optimal growth in seasonal background and ENSO cycles. Mon Weather Rev, 125: 2043–2056
Xue Y, Cane M A, Zebiak S E. 1997b. Predictability of a coupled model of ENSO using singular vector analysis. Part II: Optimal growth and forecast skill. Mon Weather Rev, 125: 2057–2073
Yu Y, Duan W, Xu H, Mu M. 2009. Dynamics of nonlinear error growth and season-dependent predictability of El Nino events in the Zebiak-Cane model. Q J R Meteorol Soc, 135: 2146–2160
Yu Y, Mu M, Duan W, Gong T. 2012. Contribution of the location and spatial pattern of initial error to uncertainties in El Niño predictions. J Geophys Res, 117: C06018
Yu Y, Mu M, Duan W. 2012. Does model parameter error cause a significant "spring predictability barrier" for el niño events in the Zebiak-Cane Model? J Clim, 25: 1263–1277
Zavala-Garay J, Moore A M, Kleeman R. 2004. Influence of stochastic forcing on ENSO prediction. J Geophys Res-Oceans, 109: C11007. doi: 10.1029/2004JC002406
Zebiak S E, Cane M A. 1987. A model El Niño-Southern Oscillation. Mon Wea Rev, 115: 2262–2278
Zhang R H, Zebiak S E, Kleeman R, Keenlyside N. 2003. A new intermediate coupled model for El Niño simulation and prediction. Geophys Res Lett, 30:153–166
Zhang R H, Zebiak S E, Kleeman R, Keenlyside N. 2005. Retrospective El Niño forecasts using an improved intermediate coupled model. Mon Wea Rev, 133: 2777–2802
Zheng F, Zhu J, Zhang R H, Zhou G Q. 2006. Ensemble hindcasts of SST anomalies in the tropical Pacific using an intermediate coupled model. Geophys Res Lett, 33: L19604
Zheng F. 2007. Researches on ENSO ensemble predictions (in Chinese). Dissertation for the Doctoral Degree. Beijing: Institute of Atmospheric Physics, Chinese Academy of Sciences
Zheng F, Zhu J, Zhang R H. 2007. Impact of altimetry data on ENSO ensemble initializations and predictions. Geophys Res Lett, 34: L13611
Zheng F, Zhu J. 2008. Balanced multivariate model errors of an intermediate coupled model for ensemble Kalman filter data assimilation. J Geophys Res, 113: 341–355
Zheng F, Zhu J, Wang H, Zhang R H. 2009a. Ensemble hindcasts of ENSO events over the past 120 years using a large number of ensembles. Adv Atmos Sci, 26: 359–372
Zheng F, Wang H, Zhu J. 2009b. ENSO ensemble prediction: Initial error perturbations vs. model error perturbations. Chin Sci Bull, 54: 2516–2523
Zheng F, Zhu J. 2010. Spring predictability barrier of ENSO events from the perspective of an ensemble prediction system. Glob Planet Change, 72: 108–117
Zheng F, Zhu J. 2010. Coupled assimilation for an intermediated coupled ENSO prediction model. Ocean Dyn, 60: 1061–1073
Zheng F, Zhu J. 2015. Roles of initial ocean surface and subsurface states on successfully predicting 2006–2007 El Niño with an intermediate coupled model. Ocean Sci, 11: 187–194
Zheng F, Zhu J. 2016. Improved ensemble-mean forecasting of ENSO events by a zero-mean stochastic error model of an intermediate coupled model. Clim Dyn, 47: 3901–3915
Zheng F, Zhu J, Zhang R H, Peng J B. 2016. Successful Prediction for the Super El Niño Event in 2015. Bull Chin Acad Sci, 31: 251–257
Zhai P, Yu R, Guo Y, Li Q, Ren X, Wang Y, Xu W, Liu Y, Ding Y. 2016. The strong El Niño of 2015/16 and its dominant impacts on global and China's climate. J Meteorol Res, 30: 283–297